

## Supporting Information for

# Hexane Isomers Separation on an Isoreticular Series of Microporous Zr Carboxylate Metal Organic Frameworks

Adriano Henrique <sup>a, b</sup>, Tanmoy Maity <sup>c</sup>, Hengli Zhao <sup>d, e</sup>, Pedro F. Brântuas <sup>b</sup>, Alírio E. Rodrigues <sup>a</sup>, Farid Nouar <sup>f</sup>, Aziz Ghoufi <sup>d</sup>, Guillaume Maurin <sup>e, \*</sup>, José A. C. Silva <sup>b, †</sup> and Christian Serre <sup>f, ‡</sup>

<sup>a</sup> *Laboratory of Separation and Reaction Engineering - Laboratory of Catalysis and Materials (LSRE/LCM), Department of Chemical Engineering, Faculty of Engineering University of Porto, Rua Dr. Roberto Frias, S/N, 4200-465 Porto, Portugal*

<sup>b</sup> *Centro de Investigação de Montanha (CIMO), Instituto Politécnico de Bragança, Campus de Santa Apolónia, 5300-253 Bragança, Portugal*

<sup>c</sup> *Solid State and Structural Chemistry Unit, Indian Institute of Science, Bangalore, Karnataka 560012, India*

<sup>d</sup> *Univ. Rennes, CNRS, IPR (Institut de Physique de Rennes) - UMR 6251, F-35000 Rennes, France*

<sup>e</sup> *ICGM, Univ. Montpellier, CNRS, ENSCM, Montpellier, France*

<sup>f</sup> *Institut des Matériaux Poreux de Paris, Ecole Normale Supérieure de Paris, ESPCI Paris, CNRS, PSL university, 75005 Paris, France*

---

\* **Corresponding author:** e-mail: [guillaume.maurin1@umontpellier.fr](mailto:guillaume.maurin1@umontpellier.fr)

† **Corresponding author:** e-mail: [jsilva@ipb.pt](mailto:jsilva@ipb.pt)

‡ **Corresponding author:** e-mail: [christian.serre@ens.fr](mailto:christian.serre@ens.fr)

## **Supporting Information File**

S1. CHARACTERIZATION OF MIL-140s .....	3
S1.1. Powder X-Ray Diffraction.....	3
S1.2. Infrared Spectroscopy .....	5
S1.3. Thermogravimetric Analysis .....	7
S1.4. Gas sorption study.....	9
S1.5. Surface Study on MIL-140B.....	13
S2. SAMPLING OF MIL-140s .....	14
S3. SIMULATIONS DETAILS AND RESULTS .....	15
S3.1. Force Field: Alkane Model .....	15
S3.2. MIL-140B Model.....	17
S3.3. Grand Canonical Monte Carlo Simulations .....	18
S3.4. Adsorption Isotherms and Radial Distribution Functions .....	19
S4. EXPERIMENTAL CONDITIONS FOR MEASURING BREAKTHROUGH CURVES OF HEXANE ISOMERS ON MIL-140s .....	24
S5. MULTICOMPONENT BREAKTHROUGH CURVES OF HEXANE ISOMERS ON MIL-140B .....	28
S6. SELECTIVITIES OF HEXANE ISOMERS ON MIL-140B .....	31
S7. IMPACT OF THE PORE SIZE .....	32
REFERENCES .....	33

## S1. CHARACTERIZATION OF MIL-140s

For the characterization of MOFs MIL-140 (A, B, and C) several physical measurements were performed: powder x-ray diffraction (PXRD), Fourier transformed infrared spectroscopy (FTIR), thermogravimetric analysis (TGA), and gas adsorption study.

The PXRD patterns of the samples were recorded with a Bruker AXS D8 ADVANCE diffractometer using  $\lambda\text{Cu K}\alpha 1,2$  radiation. FTIR spectra of powdered materials were measured on a Perkin-Elmer Spectrum 100 spectrometer under ATR technique. Thermogravimetric analysis was performed on a Mettler Toledo TGA2 unit under  $\text{N}_2$  atmosphere at  $5 \text{ K}.\text{min}^{-1}$  rate. Nitrogen adsorption isotherms at 77 K and pressure range of 0 –  $10^5$  Pa were measured using a micromeritics TriStar II Plus gas sorption system. A sample of ~ 50 mg material was introduced into an analysis tube and were evacuated under dynamic vacuum at desired temperature using micromeritics Smart VacPrep high vacuum pump. Prior to the sorption experiments, the samples were out gassed at the desired temperature (393 K) for 5 h under vacuum. For the evaluation of the pore sizes distribution of MIL-140s, the Horvath-Kawazoe method (Slit Pore Geometry) was applied.

### *S1.1. Powder X-Ray Diffraction*

The powder x-ray diffraction patterns of MIL-140s are illustrated in Figure S1.1, showing their characteristic bragg peaks. It is clear from this Figure that the sample synthesized corresponds to MIL-140 A, B, and C forms. Comparison of synthesized materials with simulated powder pattern (black, extract from .cif) suggest that the purity and quality of MIL-140s are very good and also match with reported pattern<sup>1</sup>.

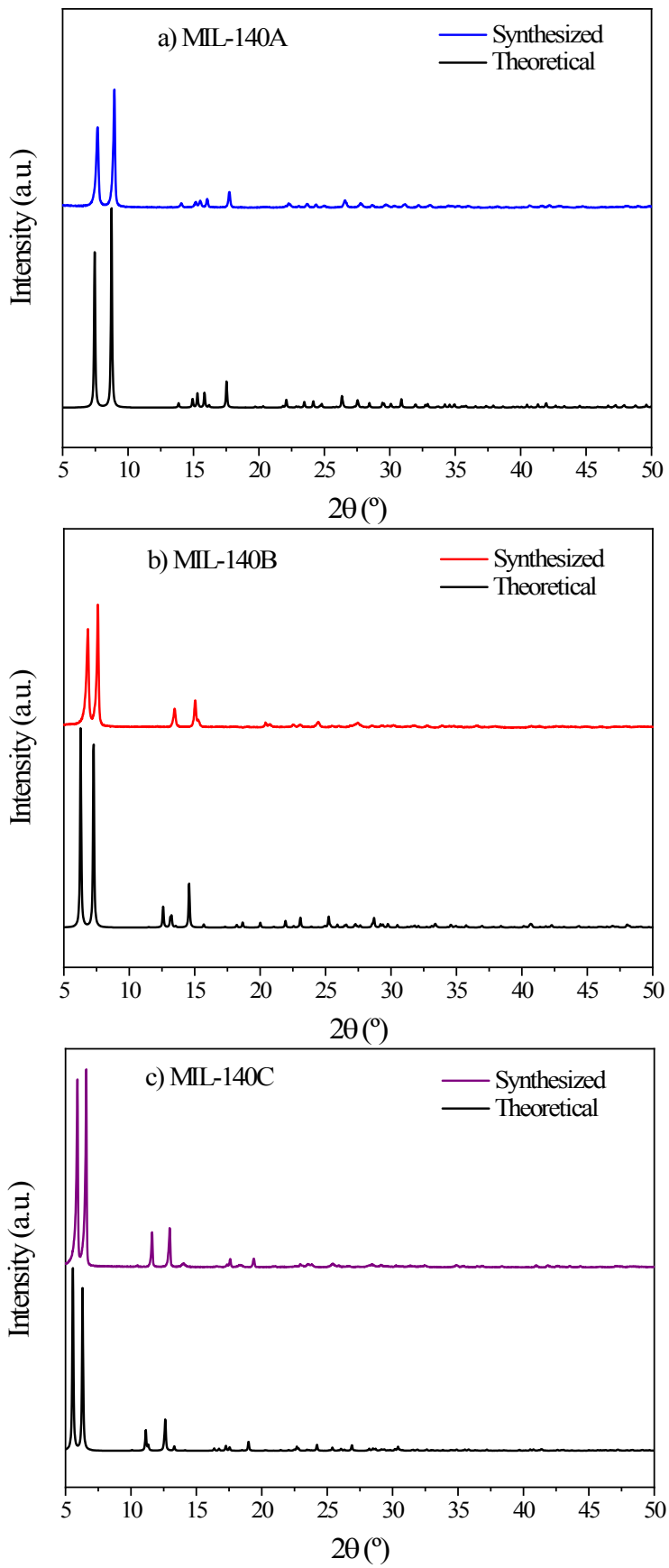


Figure S1.1. PXRD patterns of: a) MIL-140A, b) MIL-140B, and c) MIL-140C.

### **S1.2. Infrared Spectroscopy**

Fourier transformed infrared spectroscopy of materials are shown in Figure S1.2. FTIR spectra of both linker ( $\text{H}_2\text{BDC}$ ,  $\text{H}_2\text{BPDC}$  and  $\text{H}_2\text{BPDC}$  for MIL 140A, B and C, respectively) and MOF reveals that there is no presence of unreacted solid linker inside the synthesized MOF. Also the data is well matched with reported data<sup>1</sup>. Characteristics bands are visible at:

- MIL-140A: 1660, 1535, 1506, 1378, 1255, 1162, 1097, 1022, 883, 825, 743 and 660  $\text{cm}^{-1}$ ;
- MIL-140B: 1606, 1540, 1490, 1409, 1361, 1205, 1143, 923 and 783  $\text{cm}^{-1}$ ;
- MIL-140C: 1573, 1507, 1400, 1180, 1109, 849, 763 and 680  $\text{cm}^{-1}$ .

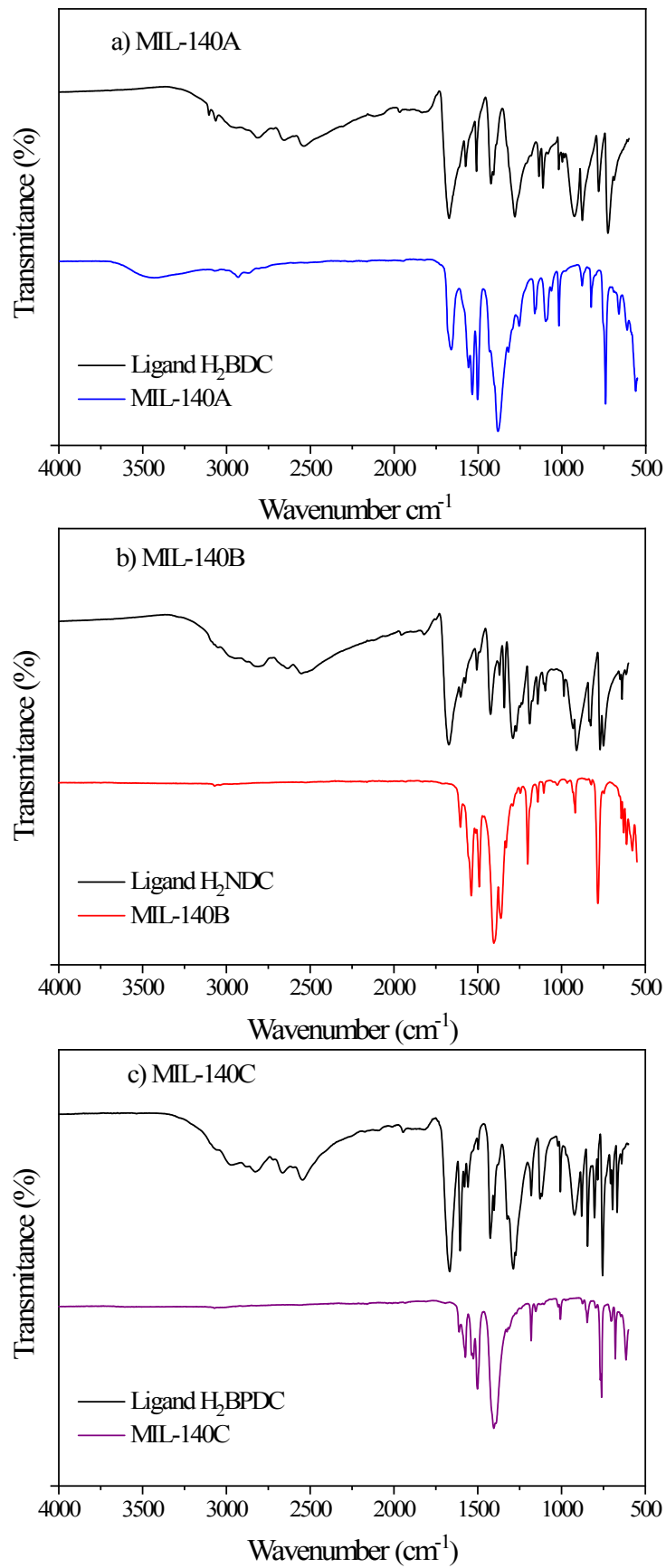


Figure S1.2. FTIR spectra of: a) MIL-140A, b) MIL-140B, and C) MIL-140C.

### **S1.3. Thermogravimetric Analysis**

Figure S1.3 revels the thermogravimetric analysis under oxygen atmosphere of MIL-140A, B, and C respectively (heating rate of 3°C/min). The TG measurements confirms that the three materials are thermally stable up to 720 K, and then shows a big mass loss due to decomposition of linker. The experimental sharp mass loss of each material is:

- MIL-140A: ~51.3% (theoretical 54.5 %);
- MIL-140B: ~52.1% (theoretical 65.2 %);
- MIL-140C: ~59.7% (theoretical 68.2 %).

The ultrahigh stability of MIL-140s mainly comes from the strong coordinative interactions between Zr(IV) ions of high charge density and the oxygen atoms of organic linkers<sup>1</sup>.

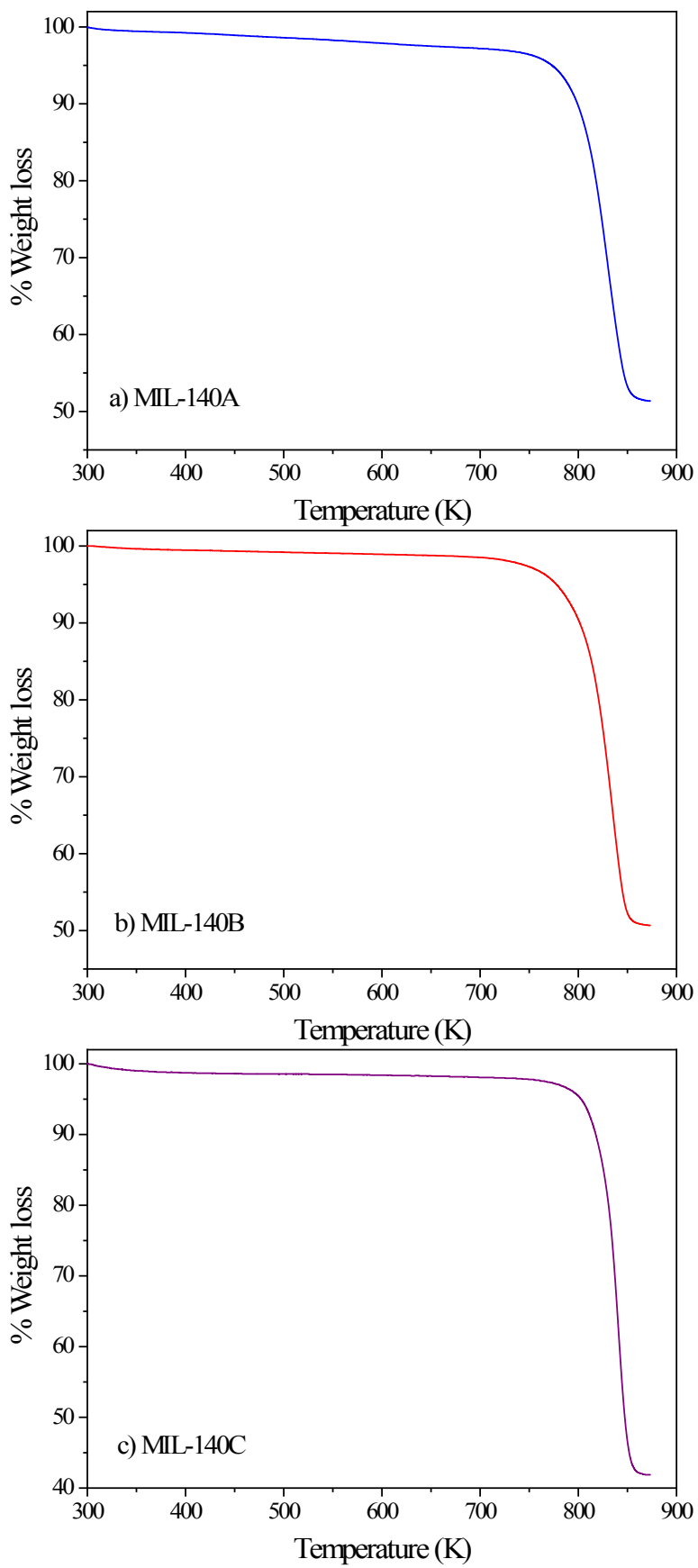


Figure S1.3. TGA analysis of: a) MIL-140A, b) MIL-140B and c) MIL-140C.

#### **S1.4. Gas sorption study**

Gas sorption measurements were undertaken to understand the porous nature of MIL-140s synthesized materials. Figure S1.4 shows the N<sub>2</sub> adsorption and desorption isotherms at 77 K on MIL-140s (outgassed at 250°C under secondary overnight), while Figure S1.5 shows the cumulative pore volume. As can be seen, the N<sub>2</sub> adsorption isotherms for the three MOFs are of type I accordingly to the IUPAC classification<sup>2</sup>, wherein the isotherms are concave to the P/P<sub>0</sub> axis with the loading reaching a limiting value. Additionally, a very sharp uptake at P/P<sub>0</sub> from 10<sup>-5</sup> to 10<sup>-1</sup> is observed, which is a signature characteristic of microporous materials. Brunauer Emmett Teller (BET) model was used for surface area measurements, being the data reported on Table S1.1, which also shows the maximum pore volume of each material.

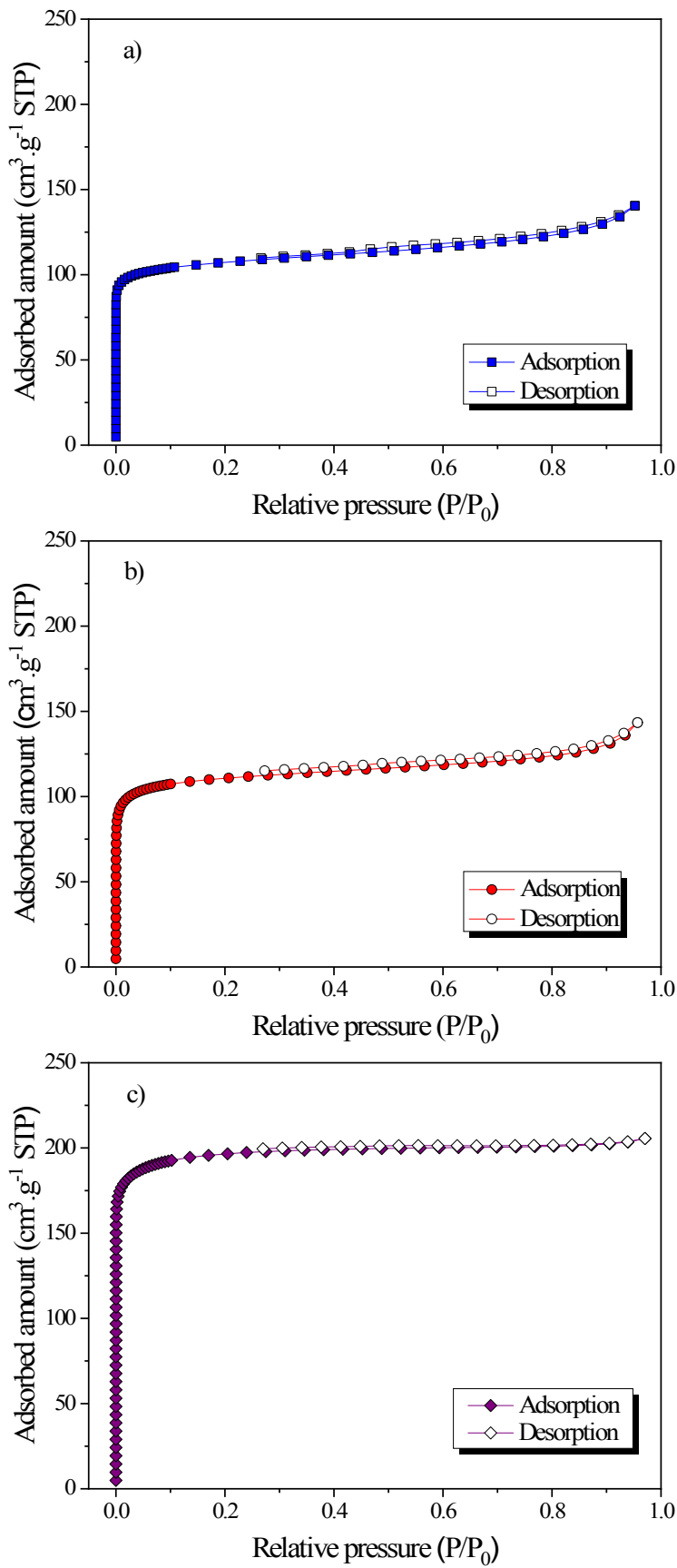


Figure S1.4. Nitrogen adsorption and desorption isotherms at 77 K on: a) MIL-140A, b) MIL-140B, and c) MIL-140C.

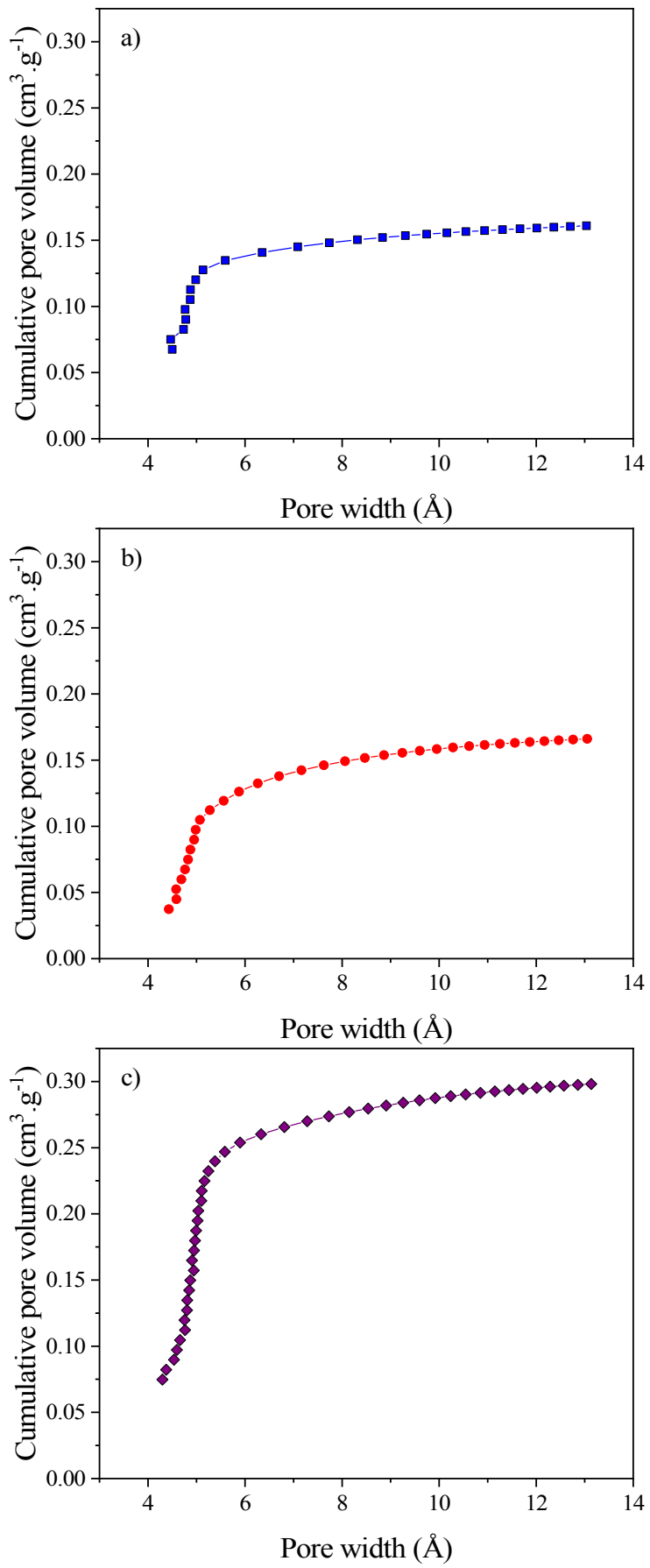


Figure S1.5. Cumulative pore volume of: a) MIL-140A, b) MIL-140B, and c) MIL-140C.

Table S1.1. Textural properties of MIL-140s

Adsorbent	S <sub>BET</sub> (m <sup>2</sup> .g <sup>-1</sup> )	Maximum pore volume (cm <sup>3</sup> .g <sup>-1</sup> )
MIL-140A	423	0.16
MIL-140B	472	0.17
MIL-140C	782	0.30

### **S1.5. Surface Study on MIL-140B**

Scanning Electron Microscopic (SEM) image (Figure S1.6) is also signifying the formation of MIL-140B with purity. The flex like shapes clearly prove the MIL-140B MOF

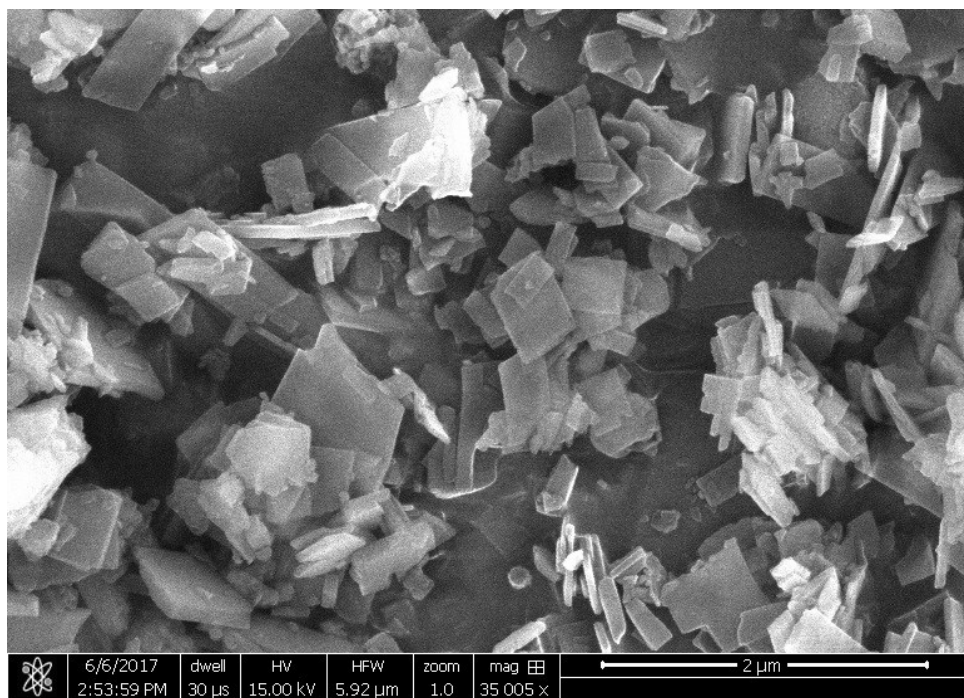


Figure S1.6. SEM image of MIL-140B.

## S2. SAMPLING OF MIL-140s

The experimental procedure used to transform the MIL-140 samples in powdered form into small agglomerates is shown in Figure S2.1.

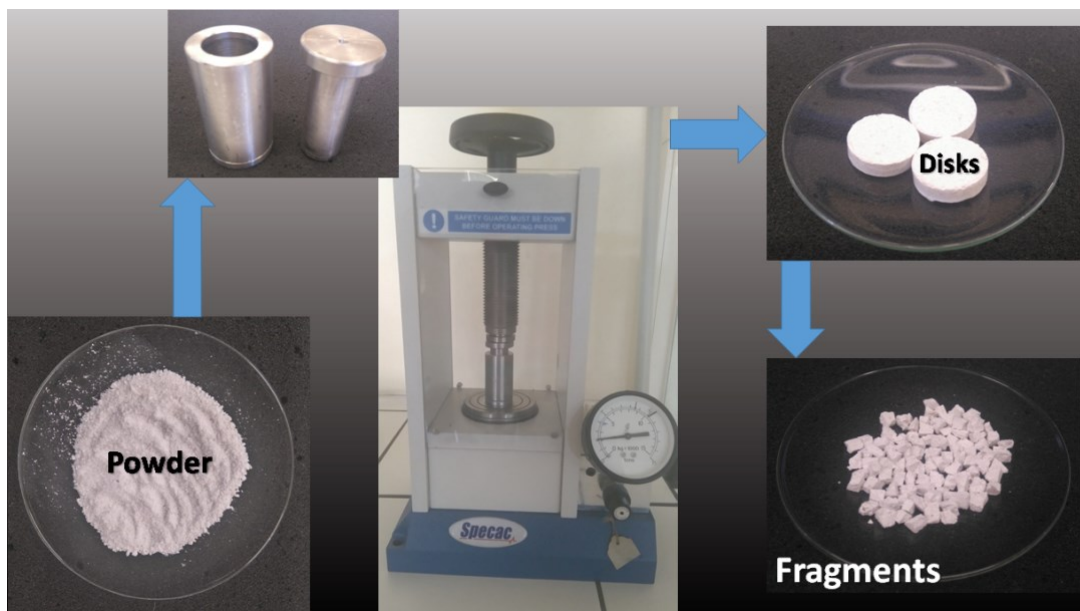


Figure S2.1. Experimental procedure for agglomeration of powdered samples of MIL-140.

### S3. SIMULATIONS DETAILS AND RESULTS

#### S3.1. Force Field: Alkane Model

TraPPE-UA<sup>3,4</sup> flexible force field was used to describe all hexane isomers, i.e. each CH<sub>x</sub> was considered as a single uncharged Lennard-Jones site.

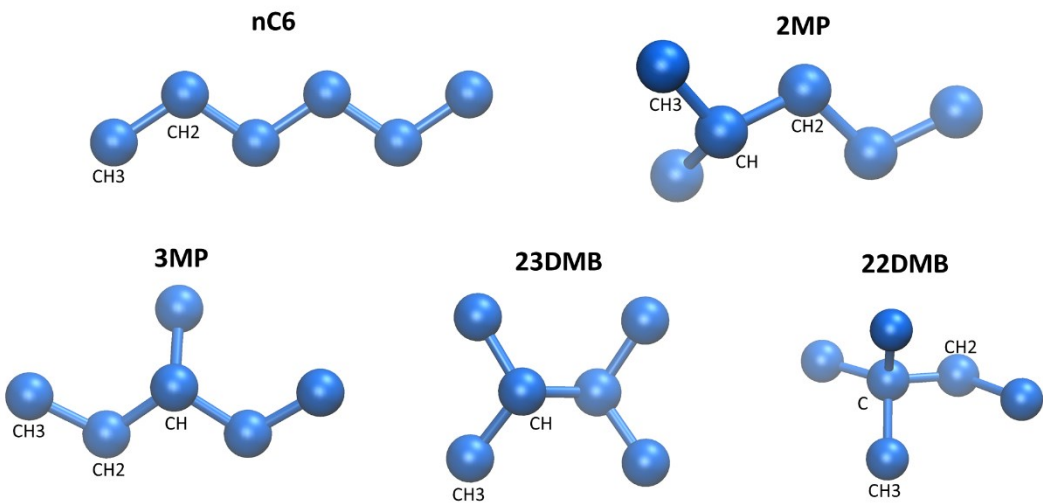


Figure S3.1. United atom models with the description of the atom types used for each hexane isomer.

In this model a harmonic cosine potential model describes the intra-molecular bond and bending contribution (equation (S3.1) and (S3.2)) while a three-cosine potential describes the torsional term ((S3.3)). LJ potential applies to the interactions between atoms separated by more than three bonds (equation (S3.4)).

$$U_{bond} = \sum_{bonds} \frac{1}{2} k_b (r - r_0)^2 \quad (\text{S3.1})$$

$$U_{bending} = \sum_{bendings} \frac{1}{2} k_\theta (\theta - \theta_0)^2 \quad (\text{S3.2})$$

$$U_{torsion} = \sum_{torsions} c_0 + c_1 [1 + \cos(\phi)] + c_2 [1 + \cos(2\phi)] + c_{13} [1 + \cos(3\phi)] \quad (\text{S3.3})$$

$$U_{ij}^{LJ} = \sum_{LJ} 4\epsilon_{ij} \left[ \left( \frac{\sigma_{ij}}{r_{ij}} \right)^{12} - \left( \frac{\sigma_{ij}}{r_{ij}} \right)^6 \right] \quad (\text{S3.4})$$

In these equations,  $k_b$  is the bond energy constant,  $r_0$  is the reference bond length,  $k_\theta$  is the bend energy constant,  $\theta_0$  is the reference bend angle.  $c_0, c_1, c_2, c_3$  are torsion parameters.  $r_{ij}$  is the distance between site i and site j.  $\sigma$  and  $\epsilon$  are LJ potential size and strength parameters respectively (see Table S3.1). The cross LJ terms between different atoms types are calculated using Lorentz-Berthelot mixing (equation (S3.5)).

$$\epsilon_{ij} = \sqrt{\epsilon_i * \epsilon_j} \quad \sigma_{ij} = \frac{\sigma_i + \sigma_j}{2} \quad (\text{S3.5})$$

Table S3.1. Intramolecular and Intermolecular potential parameters for the TraPPE-UA force field

	Stretch	$r_0$ [Å]	$k_b$ [K]
CH <sub>x</sub> -CH <sub>x</sub>	1.54	96500	

	Bendings	$\theta_0$ (°)	$k_b$ [K]
CH <sub>x</sub> -CH <sub>2</sub> -CH <sub>y</sub>	114	62500	
CH <sub>x</sub> -CH-CH <sub>y</sub>	112	62500	
CH <sub>x</sub> -C-CH <sub>y</sub>	109.47	62500	

Torsion	$c_0$ [K]	$c_1$ [K]	$c_2$ [K]	$c_3$ [K]
CH <sub>x</sub> -CH <sub>2</sub> -CH <sub>2</sub> -CHy	0	335.03	-68.19	791.32
CH <sub>x</sub> -CH <sub>2</sub> -CH-CHy	-251.06	428.73	-111.85	441.27
CH <sub>x</sub> -CH <sub>2</sub> -C-CHy	0	0	0	461.29
CH <sub>x</sub> -CH-CH-CHy	-251.06	428.73	-111.85	441.27
CH <sub>x</sub> -CH-C-CHy	0	0	0	1635.7

LJ Type	$\epsilon$ [K]	$\sigma$ [Å]
CH <sub>4</sub>	158.5	3.72
CH <sub>3</sub>	98	3.75
CH <sub>2</sub>	48	3.95
CH	10	4.8
C	0.5	6.4

### S3.2. MIL-140B Model

The crystal structure was taken from the previously reported study<sup>5</sup> All atoms of the MIL-140B were treated as single uncharged LJ sites with parameters taken from the UFF and DREIDING<sup>6,7</sup> force fields for the Zr atoms and the rest of the atoms respectively (Table S3.2).

Table S3.2. MIL-140B force field parameters

Type	$\epsilon$ [K]	$\sigma$ [ $\text{\AA}$ ]
C (DREIDING)	37.856	3.473
H (DREIDING)	7.649	2.846
O (DREIDING)	48.158	2.593
Zr (UFF)	34.7	2.783

We applied a series of linker tilting such that only the positions of atoms on the aromatic ring change (see figure S3.2).

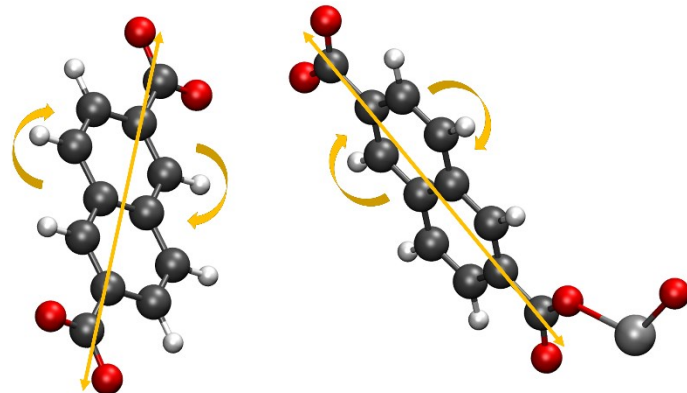


Figure S3.2. Perpendicular and orthogonal linker tilting in the unit cell. Here,  $\longleftrightarrow$  represents the axis of rotation. The carbon, hydrogen and oxygen atoms are represented in grey, white and red respectively.

### S3.3. Grand Canonical Monte Carlo Simulations

Single-component (hexane isomers) and equimolar quinary mixture adsorption isotherms were calculated by grand canonical Monte Carlo (GCMC) simulations at 343 K. These calculations were carried out using a simulation box corresponding to a 1x2x4 supercell of MIL-140B with different linker rotations (Figure S3.3). The simulation consisted of  $5 \times 10^5$  Monte Carlo steps for equilibration and  $4 \times 10^6$  Monte Carlo steps for production. Several types of Monte Carlo moves were considered in our simulation: translation move, rotation move, internal rotation move, and insertion/deletion move. The frequencies of these moves were respectively 0.3, 0.2, 0.2, and 0.3. The cutoff distance was set for 12 Å. The approximation that fugacity is equal to gas pressure for the adsorption was also adopted.

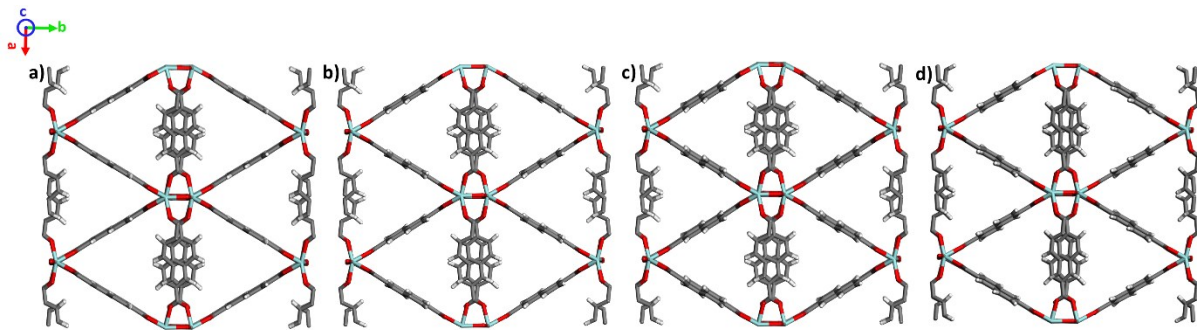


Figure S3.3. View of MIL-140B along the xy plane: pristine structure (a) and its modified version with a linker rotation of (b)  $-10^\circ$ , (c)  $-5^\circ$ , and (d)  $10^\circ$ . The carbon, hydrogen, oxygen and zirconium atoms are represented in grey, white, red and cyan respectively.

$Q_{st}$  were calculated by the following expression, with U the total energy, N the number of adsorbates, R the gas constant and T the temperature.

$$Q_{st} = RT - [\langle UN \rangle - \langle U \rangle \langle N \rangle] / [\langle N^2 \rangle - \langle N \rangle^2] \quad (\text{S3.6})$$

### S3.4. Adsorption Isotherms and Radial Distribution Functions

Single component adsorption isotherms on MIL-140B:

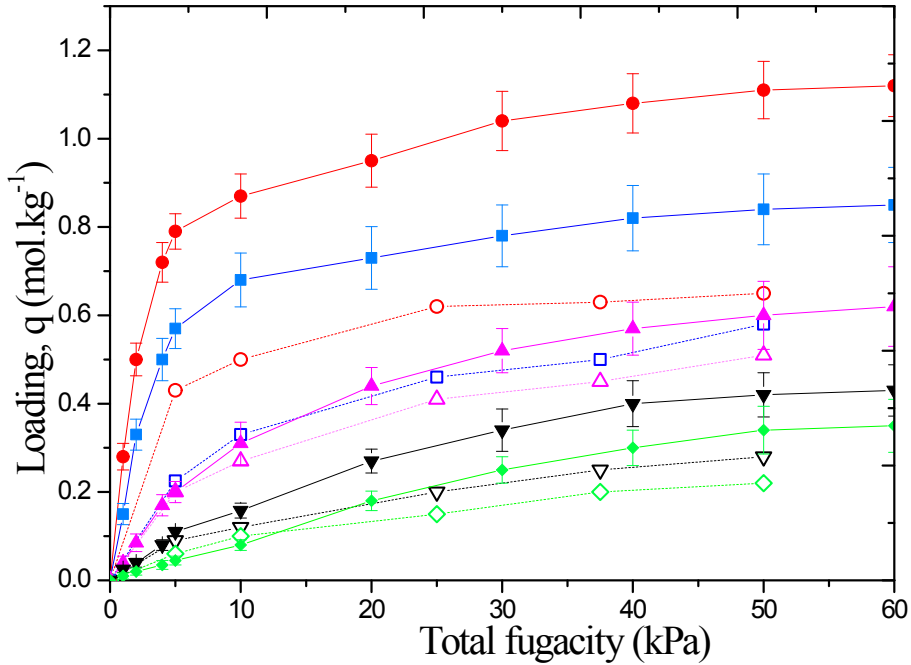


Figure S3.4. GCMC simulated single component adsorption isotherms at 343K on the pristine MIL-140B structure. The experimental data is represented by open symbols connected by dashed lines. The simulation data are represented by filled symbols connected by solid lines. -○- nC6 experimental data, -●- nC6 simulation data, -□- 2MP experimental data, -■- 2MP simulation data, -△- 3MP experimental data, -▲- 3MP simulation data, -▽- 23DMB experimental data, -▼- 23DMB simulation data, -◇- 22DMB experimental data, -◆- 22DMB simulation data.

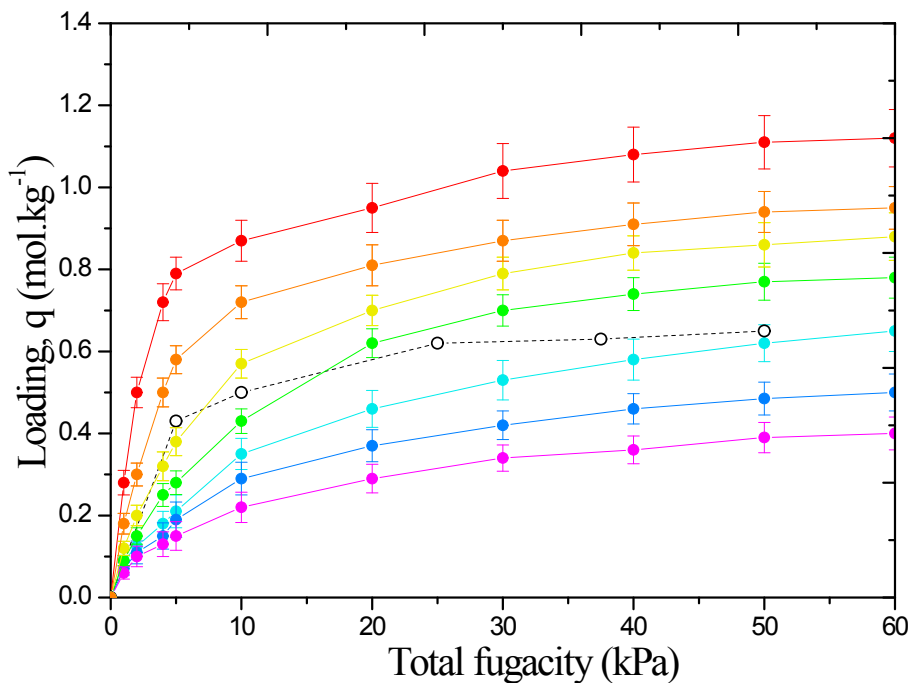


Figure S3.5. GCMC simulated nC6 isotherms at 343K on MIL-140B characterized by different linker tilting angles. -○- experimental data, -●- 0° linker rotation, -○- 2° linker rotation, -○- 5° linker rotation, -○- 7° linker rotation, -○- 10° linker rotation, -○- 12° linker rotation, -○- 15° linker rotation.

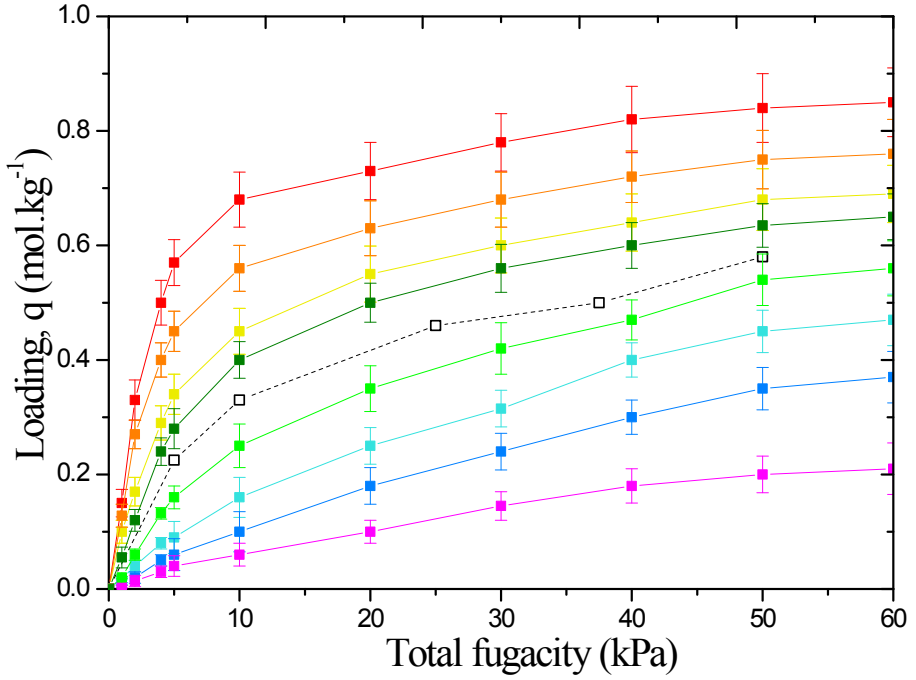


Figure S3.6. GCMC simulated 2MP isotherms at 343K on MIL-140B characterized by different linker tilting angles.  
- □- experimental data, -■- 0° linker rotation, -■- 2° linker rotation, -■- 5° linker rotation, -■- 6° linker rotation, -■- 7° linker rotation, -■- 10° linker rotation, -■- 12° linker rotation, -■- 15° linker rotation.

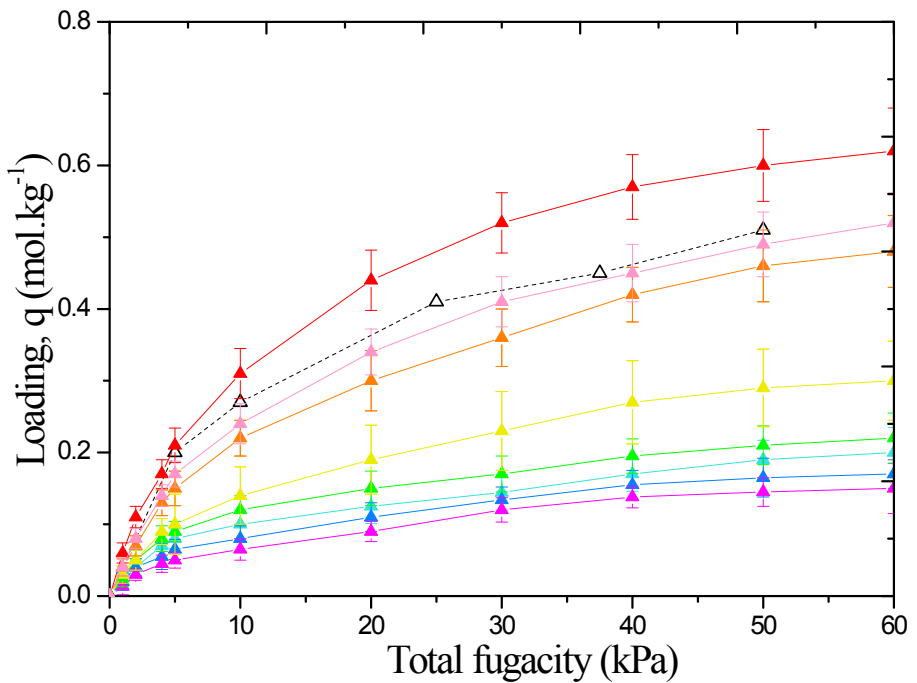


Figure S3.7. GCMC simulated 3MP isotherms at 343K on MIL-140B characterized by different linker tilting angles.  
-△- experimental data, -▲- 0° linker rotation, -▲- 1° linker rotation, -▲- 2° linker rotation, -▲- 5° linker rotation, -▲- 7° linker rotation, -▲- 10° linker rotation, -▲- 12° linker rotation, -▲- 15° linker rotation.

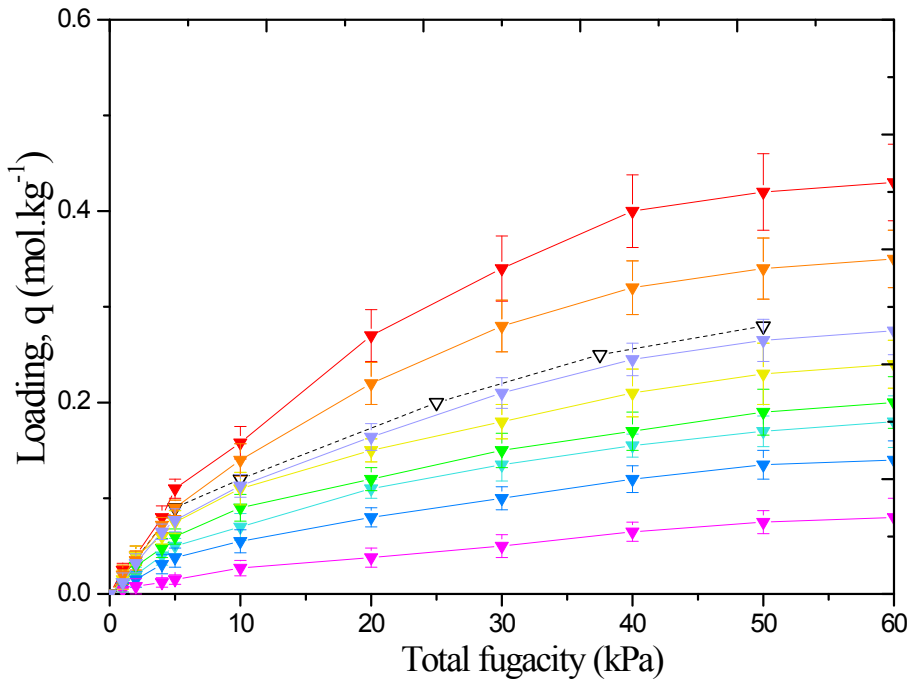


Figure S3.8. GCMC simulated 23 DMB isotherms at 343K on MIL-140B characterized by different linker tilting angles. - $\nabla$ - experimental data, - $\blacktriangledown$ - 0° linker rotation, - $\blacktriangledown$ - 2° linker rotation, - $\blacktriangledown$ - 4° linker rotation, - $\blacktriangledown$ - 5° linker rotation, - $\blacktriangledown$ - 7° linker rotation, - $\blacktriangledown$ - 10° linker rotation, - $\blacktriangledown$ - 12° linker rotation, - $\blacktriangledown$ - 15° linker rotation.

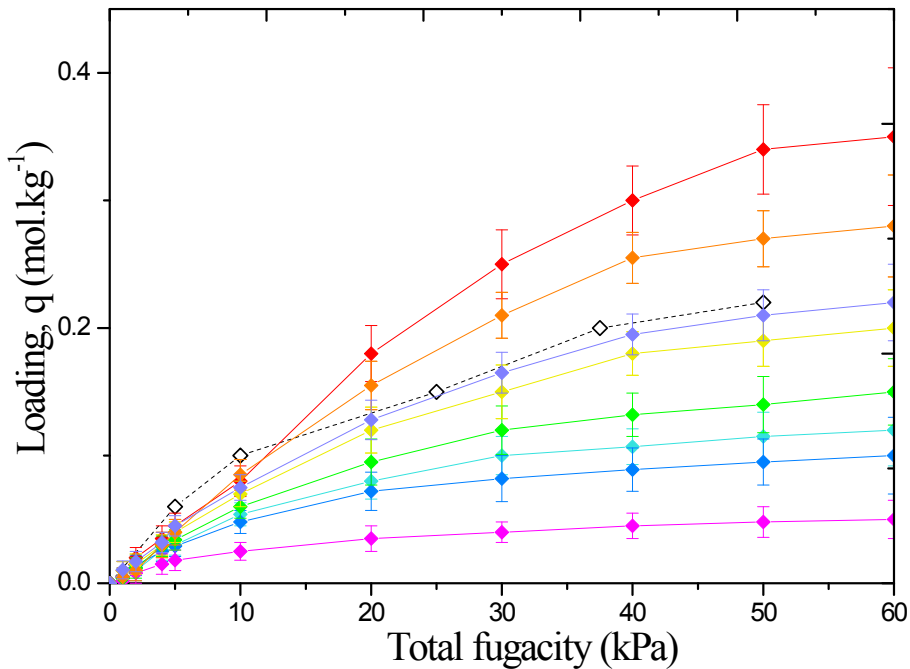


Figure S3.9. GCMC simulated 22 DMB isotherms at 343K on MIL-140B characterized by different linker tilting angles. - $\diamond$ - experimental data, - $\blacklozenge$ - 0° linker rotation, - $\blacklozenge$ - 2° linker rotation, - $\blacklozenge$ - 4° linker rotation, - $\blacklozenge$ - 5° linker rotation, - $\blacklozenge$ - 7° linker rotation, - $\blacklozenge$ - 10° linker rotation, - $\blacklozenge$ - 12° linker rotation, - $\blacklozenge$ - 15° linker rotation.

Multicomponent adsorption isotherms on MIL-140B:

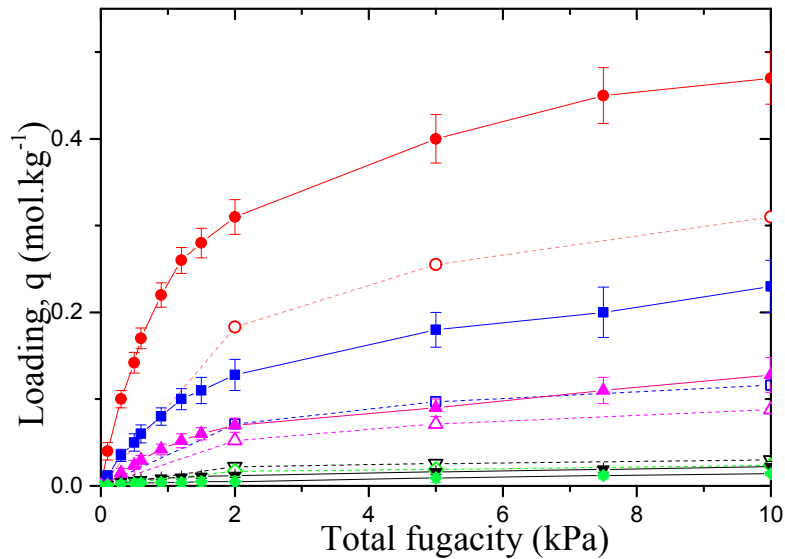


Figure S3.10. Equimolar quinary mixture adsorption isotherms at 343K on the pristine MIL-140B. The experimental data is represented by open symbol connected by dash line. The simulation data is represented by filled symbol connected by solid line. ■■■ nC6 experimental data, ■■■ nC6 simulation data, ■■■ 2MP experimental data, ■■■ 2MP simulation data, ■■■ 3MP experimental data, ■▲■ 3MP simulation data ■■■ 23DMB experimental data, ■■■ 23DMB simulation data ■■■ 22DMB experimental data, ■■■ 22DMB simulation data.

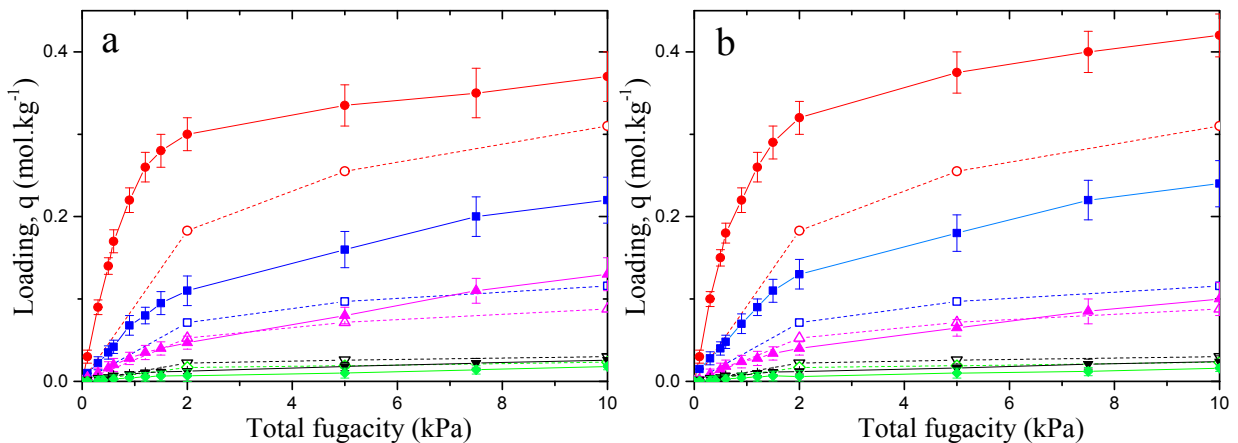


Figure S3.11: a) Equimolar quinary mixture adsorption isotherms at 343K on the MIL-140B characterized by a tilting angle of 10°, and b) Equimolar quinary mixture adsorption isotherms at 343K on MIL-140B characterized by a tilting angle of 7°. The experimental data is represented by open symbol connected by dash line. The simulation data is represented by filled symbol connected by solid line. ■■■ nC6 experimental data, ■■■ nC6 simulation data, ■■■ 2MP experimental data, ■■■ 2MP simulation data, ■■■ 3MP experimental data, ■■■ 3MP simulation data ■■■ 23DMB experimental data, ■■■ 23DMB simulation data, ■■■ 22DMB experimental data, ■■■ 22DMB simulation data.

### Radial Distribution Functions:

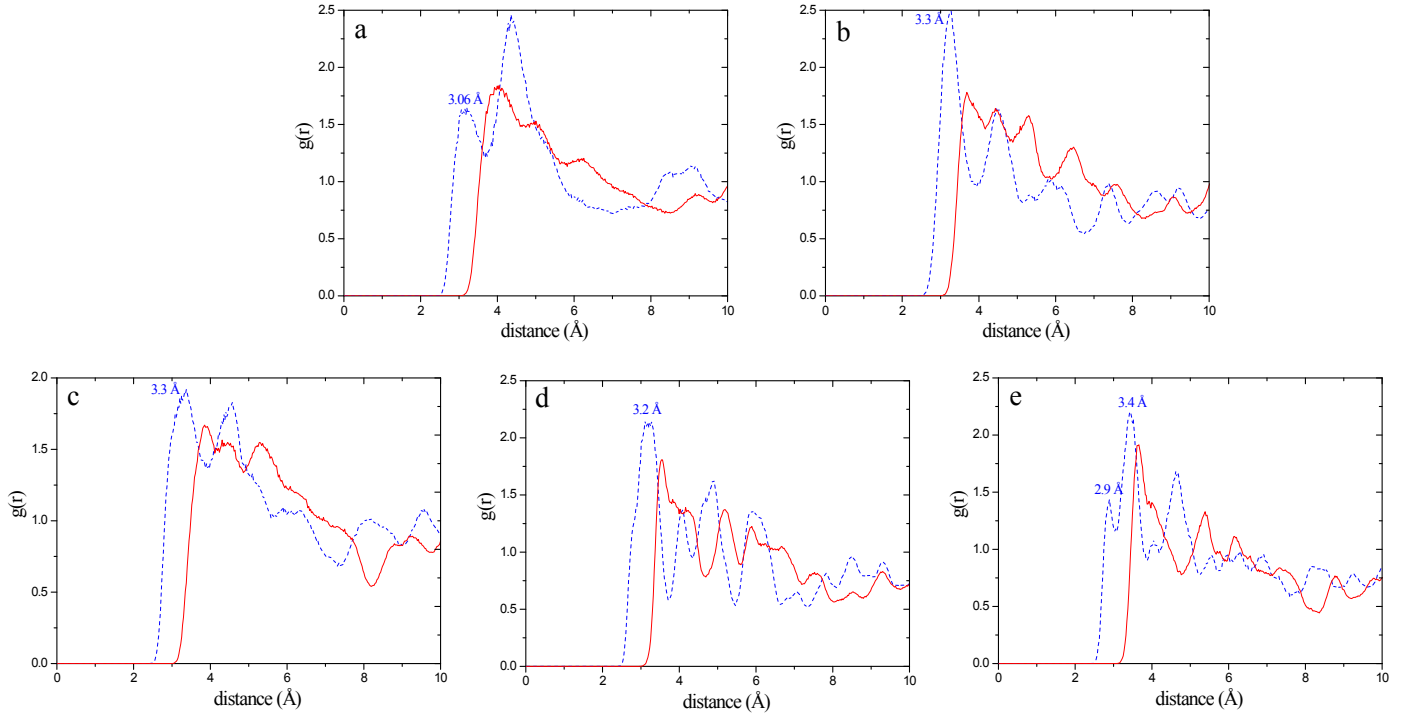


Figure S3.12: Most representative RDF plotted between MOF/hexane isomer pairs RDF between CH<sub>3</sub>(UA) and H from MIL-140B aromatic ring is represented in blue dash line. The RDF between CH<sub>3</sub>(UA) and C from MIL-140B aromatic ring is represented in black solid line. The figure a), b), c), d), and e) represent the case of adsorption of nC<sub>6</sub>, 2MP, 3MP, 23DMB, and 22DMB respectively. The loading for nC<sub>6</sub>, 2MP and 3MP correspond to 1 molecule per unit cell. The loading for 22DMB and 23DMB corresponds to 0.5 molecule per unit cell. The MIL-140B linker tilting for nC<sub>6</sub>, 2MP, 3MP, 23DMB, and 22DMB were 10°, 7°, 2°, 4°, and 4°.

#### S4. EXPERIMENTAL CONDITIONS FOR MEASURING BREAKTHROUGH CURVES OF HEXANE ISOMERS ON MIL-140s

Table S4.1. Experimental conditions for measuring single component breakthrough curves of hexane isomers on MIL-140B and loadings.

Run	Temperature (K)	Total hydrocarbon pressure (kPa)	Paraffin flowrate* ( $\mu\text{mol} \cdot \text{min}^{-1}$ )	Helium flowrate* ( $\text{mL} \cdot \text{min}^{-1}$ )	Loading ( $\text{mol} \cdot \text{kg}^{-1}$ )
<i>nC<sub>6</sub></i>					
1_1	343	5.00	11.6	5.00	0.418
1_2	343	10.0	24.5	5.00	0.491
1_3	343	25.0	40.5	2.76	0.617
1_4	343	37.0	59.9	2.32	0.637
1_5	343	50.0	81.0	1.84	0.664
1_6	373	5.00	11.6	5.00	0.216
1_7	373	10.0	24.5	5.00	0.330
1_8	373	25.0	40.5	2.76	0.411
1_9	373	37.0	59.9	2.32	0.447
1_10	373	50.0	81.0	1.84	0.515
1_11	423	5.00	11.6	5.00	0.107
1_12	423	10.0	24.5	5.00	0.137
1_13	423	25.0	40.5	2.76	0.199
1_14	423	37.0	59.9	2.32	0.232
1_15	423	50.0	81.0	1.84	0.256
<i>2MP</i>					
2_1	343	5.00	11.6	5.00	0.229
2_2	343	10.0	24.5	5.00	0.329
2_3	343	25.0	40.5	2.76	0.468
2_4	343	37.0	59.9	2.32	0.499
2_5	343	50.0	81.0	1.84	0.574
2_6	373	5.00	11.6	5.00	0.114
2_7	373	10.0	24.5	5.00	0.176
2_8	373	25.0	40.5	2.76	0.267
2_9	373	37.0	59.9	2.32	0.331
2_10	373	50.0	81.0	1.84	0.404
2_11	423	5.00	11.6	5.00	0.0505
2_12	423	10.0	24.5	5.00	0.0885
2_13	423	25.0	40.5	2.76	0.109
2_14	423	37.0	59.9	2.32	0.146
2_15	423	50.0	81.0	1.84	0.178

*Continued on next page*

Run	Temperature (K)	Total hydrocarbon pressure (kPa)	Paraffin flowrate* ( $\mu\text{mol}.\text{min}^{-1}$ )	Helium flowrate* ( $\text{mL}.\text{min}^{-1}$ )	Loading ( $\text{mol}.\text{kg}^{-1}$ )
<i>3MP</i>					
3_1	343	5.00	11.6	5.00	0.199
3_2	343	10.0	24.5	5.00	0.287
3_3	343	25.0	40.5	2.76	0.411
3_4	343	37.0	59.9	2.32	0.471
3_5	343	50.0	81.0	1.84	0.509
3_6	373	5.00	11.6	5.00	0.0900
3_7	373	10.0	24.5	5.00	0.134
3_8	373	25.0	40.5	2.76	0.261
3_9	373	37.0	59.9	2.32	0.275
3_10	373	50.0	81.0	1.84	0.323
3_11	423	5.00	11.6	5.00	0.0481
3_12	423	10.0	24.5	5.00	0.0651
3_13	423	25.0	40.5	2.76	0.110
3_14	423	37.0	59.9	2.32	0.138
3_15	423	50.0	81.0	1.84	0.161
<i>23DMB</i>					
4_1	343	5.00	11.6	5.00	0.0792
4_2	343	10.0	24.5	5.00	0.114
4_3	343	25.0	40.5	2.76	0.196
4_4	343	37.0	59.9	2.32	0.249
4_5	343	50.0	81.0	1.84	0.298
4_6	373	5.00	11.6	5.00	0.0508
4_7	373	10.0	24.5	5.00	0.0731
4_8	373	25.0	40.5	2.76	0.122
4_9	373	37.0	59.9	2.32	0.155
4_10	373	50.0	81.0	1.84	0.206
4_11	423	5.00	11.6	5.00	0.0272
4_12	423	10.0	24.5	5.00	0.0439
4_13	423	25.0	40.5	2.76	0.0681
4_14	423	37.0	59.9	2.32	0.0897
4_15	423	50.0	81.0	1.84	0.110
<i>22DMB</i>					
5_1	343	5.00	11.6	5.00	0.0617
5_2	343	10.0	24.5	5.00	0.0934
5_3	343	25.0	40.5	2.76	0.155
5_4	343	37.0	59.9	2.32	0.200
5_5	343	50.0	81.0	1.84	0.237
5_6	373	5.00	11.6	5.00	0.0398
5_7	373	10.0	24.5	5.00	0.0572
5_8	373	25.0	40.5	2.76	0.0943
5_9	373	37.0	59.9	2.32	0.122
5_10	373	50.0	81.0	1.84	0.153
5_11	423	5.00	11.6	5.00	0.0183
5_12	423	10.0	24.5	5.00	0.0362
5_13	423	25.0	40.5	2.76	0.0571
5_14	423	37.0	59.9	2.32	0.0751
5_15	423	50.0	81.0	1.84	0.0917

\*STP: Standard Temperature and Pressure Conditions

The mass of MIL-140B used in the experiments was 630 mg.

Table S4.2. Experimental conditions for measuring multicomponent breakthrough curves of hexane isomers on MIL-140B and loadings.

Run	Temp. (K)	Total hydrocarbon pressure (kPa)	Paraffin flowrate* ( $\mu\text{mol} \cdot \text{min}^{-1}$ )	Helium flowrate* ( $\text{mL} \cdot \text{min}^{-1}$ )	Loading ( $\text{mol} \cdot \text{kg}^{-1}$ )		Mixture loading ( $\text{mol} \cdot \text{kg}^{-1}$ )			
					22DMB	23DMB	3MP	2MP	nC6	
1_1	343	10.0	16.2	3.31	0.0163	0.0204	0.0515	0.0704	0.183	0.342
1_2	343	25.0	40.5	2.76	0.0180	0.0249	0.0704	0.0960	0.254	0.463
1_3	343	50.0	81.0	1.84	0.0221	0.0290	0.0874	0.115	0.309	0.562
2_1	373	10.0	16.2	3.31	0.0126	0.0180	0.0313	0.0394	0.0951	0.196
2_2	373	25.0	40.5	2.76	0.0165	0.0212	0.0476	0.0602	0.160	0.305
2_3	373	50.0	81.0	1.84	0.0191	0.0263	0.0578	0.0734	0.194	0.371
3_1	423	10.0	16.2	3.31	0.0102	0.0120	0.0155	0.0161	0.0313	0.0850
3_2	423	25.0	40.5	2.76	0.0143	0.0169	0.0271	0.0287	0.0523	0.139
3_3	423	50.0	81.0	1.84	0.0176	0.0218	0.0313	0.0342	0.0710	0.176

\*STP: Standard Temperature and Pressure Conditions

The mass of MIL-140B used in the experiments was 650 mg.

Table S4.3. Experimental conditions for measuring multicomponent breakthrough curves of hexane isomers on MIL-140s and loadings.

Run	Temp. (K)	Total hydrocarbon pressure (kPa)	Paraffin flowrate* ( $\mu\text{mol} \cdot \text{min}^{-1}$ )	Helium flowrate* ( $\text{mL} \cdot \text{min}^{-1}$ )	Mass of adsorbent (mg)	Loading ( $\text{mol} \cdot \text{kg}^{-1}$ )				Mixture loading ( $\text{mol} \cdot \text{kg}^{-1}$ )	
2_1A	343	10.0	16.2	3.31	614	0.0383	0.0538	0.0656	0.0625	0.0826	0.303
2_2A	343	25.0	40.5	2.76	614	0.0461	0.0654	0.0802	0.0754	0.102	0.369
2_3A	343	50.0	81.0	1.84	614	0.0730	0.0724	0.0921	0.0851	0.126	0.448
2_1B	343	10.0	16.2	3.31	650	0.0163	0.0204	0.0515	0.0704	0.183	0.342
2_2B	343	25.0	40.5	2.76	650	0.0180	0.0249	0.0704	0.0960	0.254	0.463
2_3B	343	50.0	81.0	1.84	650	0.0221	0.0290	0.0874	0.115	0.309	0.562
2_1C	343	10.0	16.2	3.31	536	0.228	0.280	0.359	0.296	0.359	1.52
2_2C	343	25.0	40.5	2.76	536	0.233	0.284	0.361	0.297	0.318	1.49
2_3C	343	50.0	81.0	1.84	536	0.247	0.284	0.376	0.304	0.332	1.54

\*STP: Standard Temperature and Pressure Conditions

**S5. MULTICOMPONENT BREAKTHROUGH CURVES OF HEXANE ISOMERS ON MIL-140B**

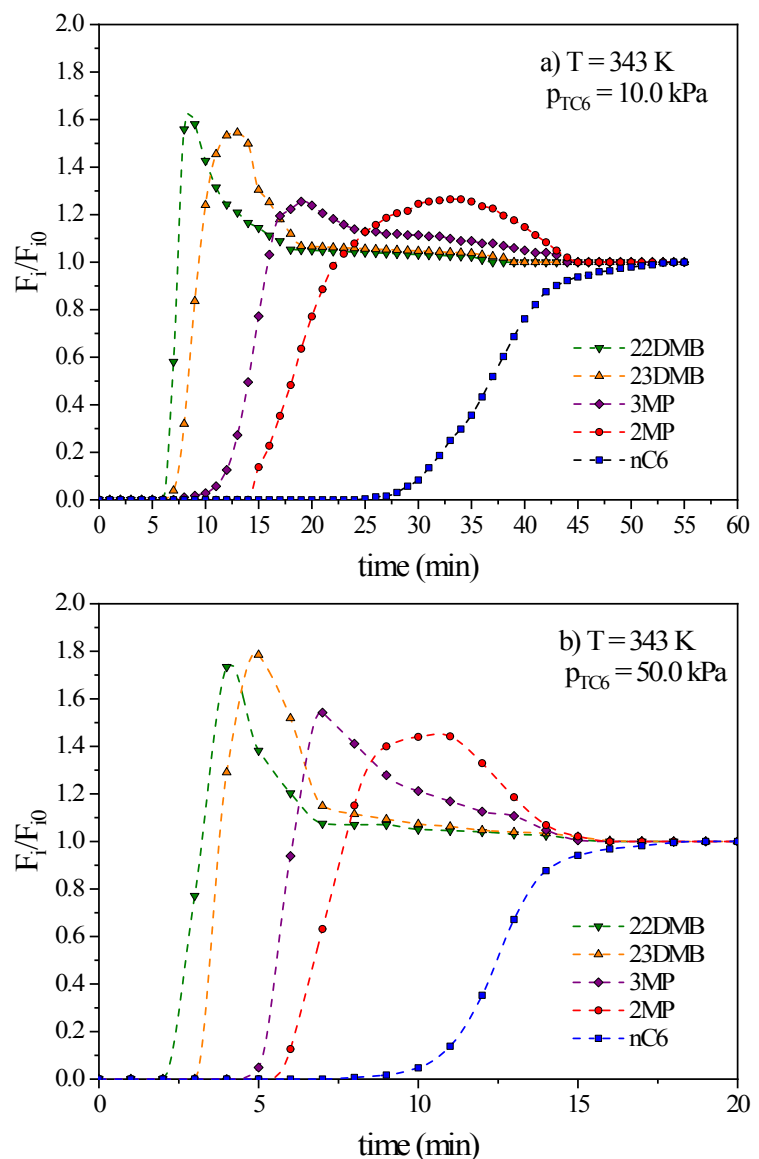


Figure S5.1. Multicomponent breakthrough curves for a quinary equimolar mixture of hexane isomers on MIL-140B at 343 K and total hydrocarbon pressure of: a) 10.0 kPa and b) 50.0 kPa.

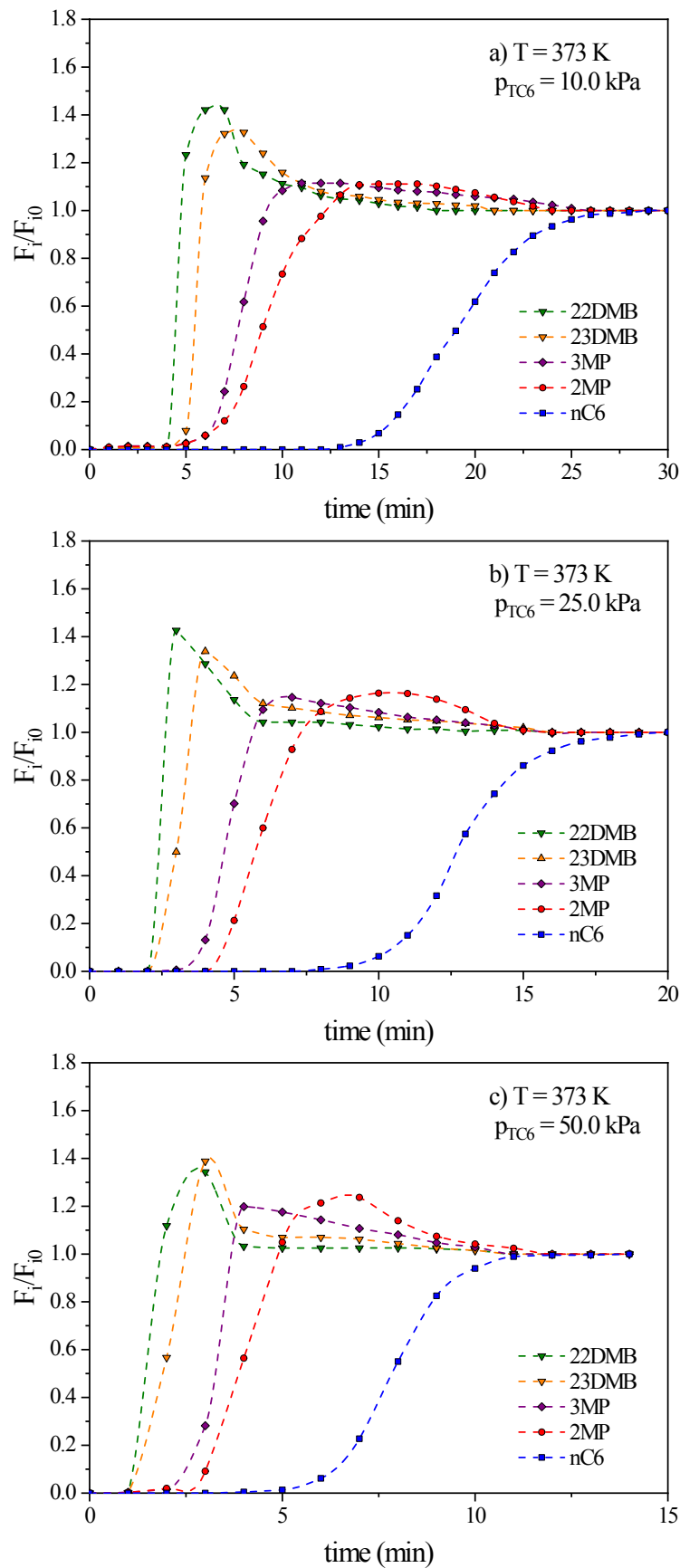


Figure S5.2. Multicomponent breakthrough curves for a quinary equimolar mixture of hexane isomers on MIL-140B at 373 K and total hydrocarbon pressure of: a) 10.0 kPa, b) 25.0 kPa, and c) 50.0 kPa.

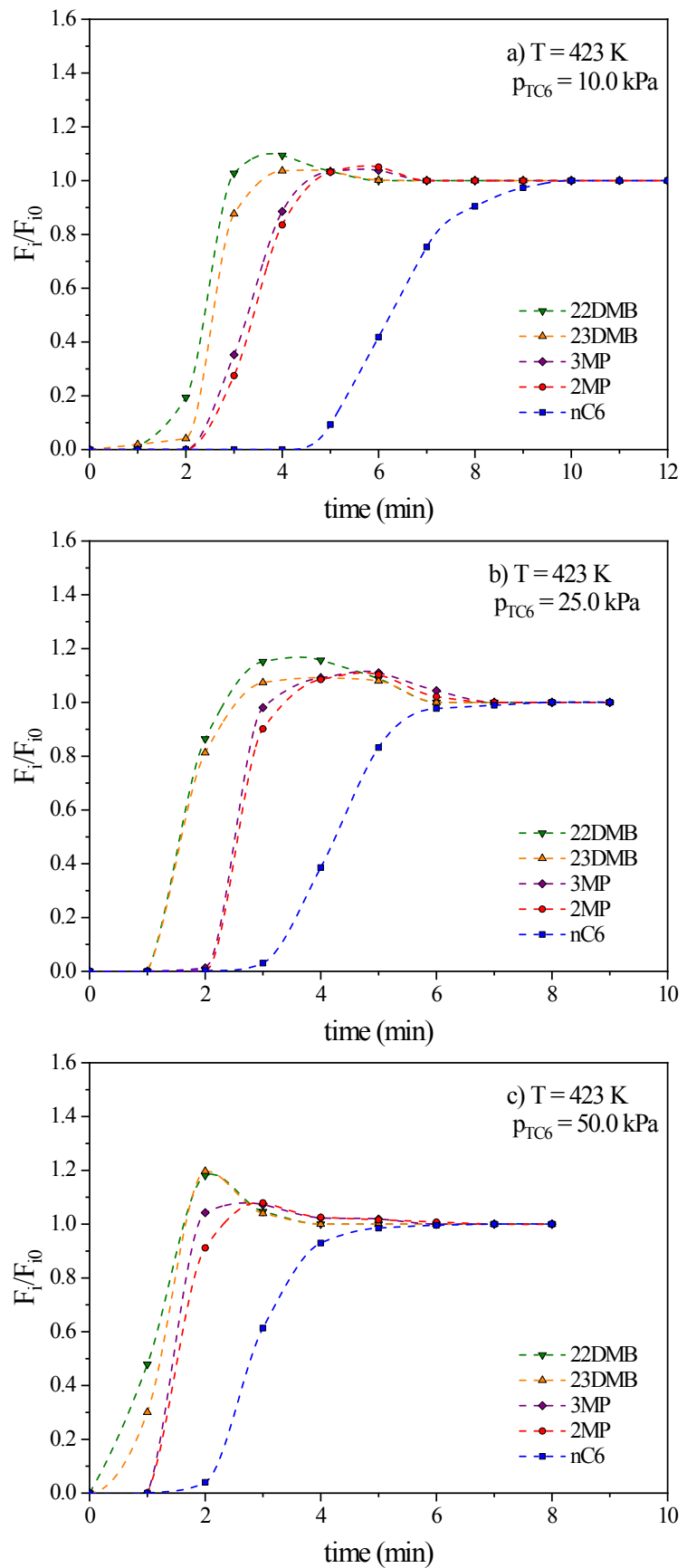


Figure S5.3. Multicomponent breakthrough curves for a quinary equimolar mixture of hexane isomers on MIL-140B at 423 K and total hydrocarbon pressure of: a) 10.0 kPa, b) 25.0 kPa, and c) 50.0 kPa.

## S6. SELECTIVITIES OF HEXANE ISOMERS ON MIL-140B

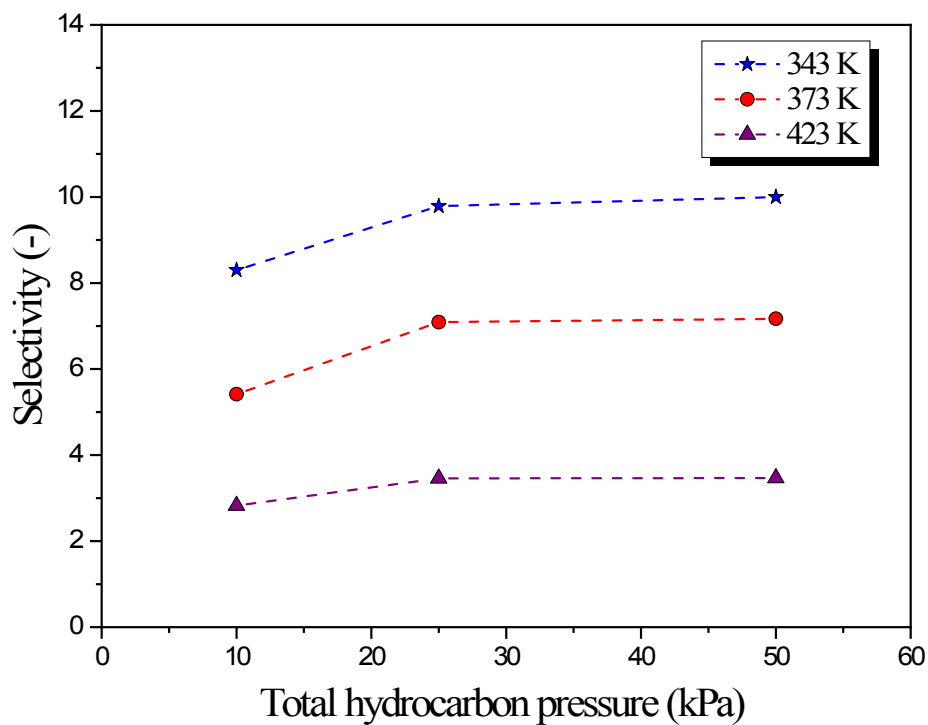


Figure S6.1. Multicomponent sorption selectivities of hexane isomers on MIL-140B as a function of total hydrocarbon pressure at: a) 343 K, b) 373 K, and c) 423 K.

## S7. IMPACT OF THE PORE SIZE

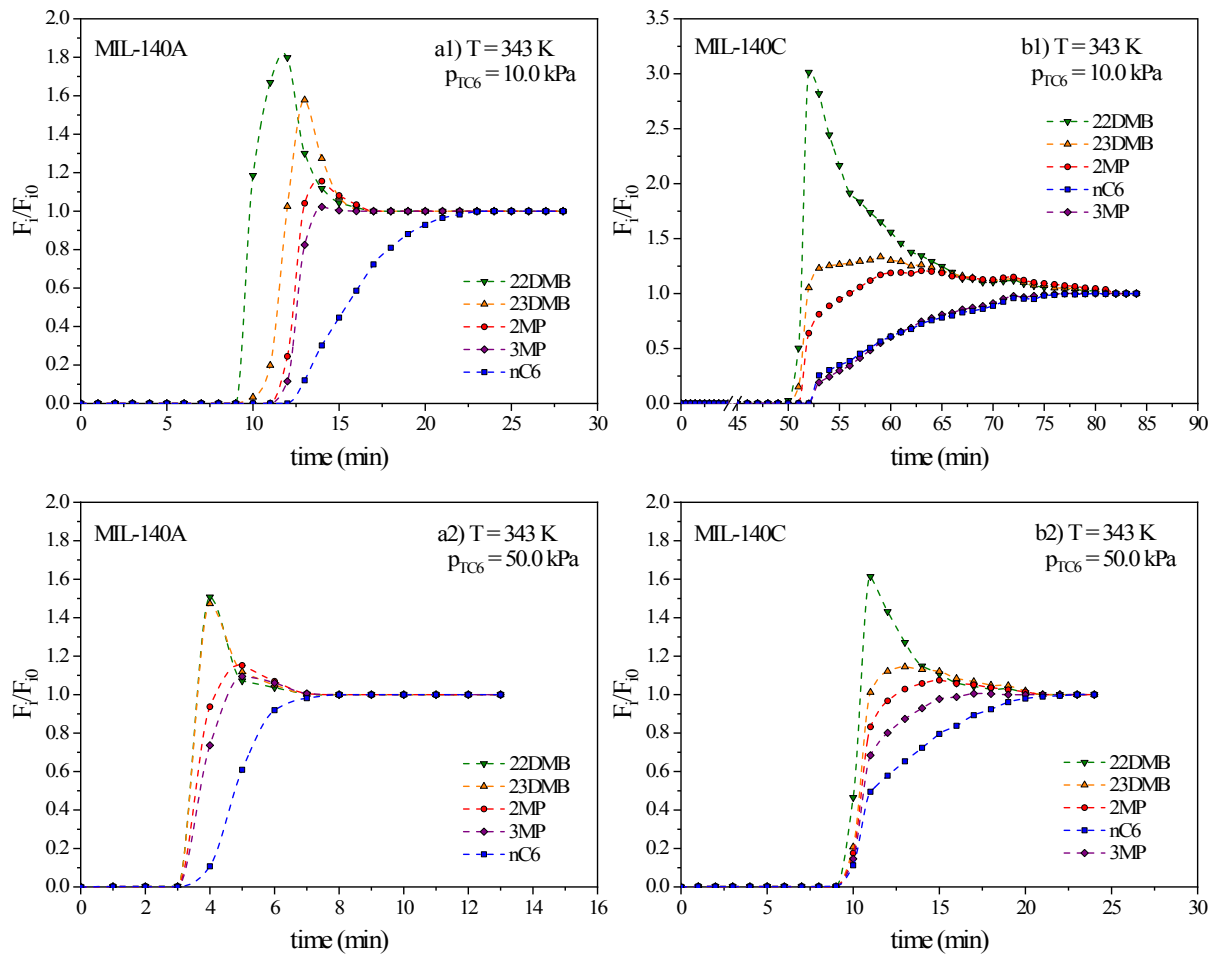


Figure S7.1. Experimental multicomponent breakthrough curves for a quinary equimolar mixture of hexane isomers on: a) MIL-140A and b) MIL-140C. Temperature of 343 K and total hydrocarbon pressure of: 1) 10.0 kPa and 2) 50.0 kPa.

## REFERENCES

- 1 V. Guillerm, F. Ragon, M. Dan-Hardi, T. Devic, M. Vishnuvarthan, B. Campo, A. Vimont, G. Clet, Q. Yang, G. Maurin, G. Férey, A. Vittadini, S. Gross and C. Serre, *Angew. Chemie - Int. Ed.*, 2012, **51**, 9267–9271.
- 2 M. Thommes, K. Kaneko, A. V. Neimark, J. P. Olivier, F. Rodriguez-Reinoso, J. Rouquerol and K. S. W. Sing, *Pure Appl. Chem.*, 2015, **87**, 1051–1069.
- 3 M. G. Martin and J. I. Siepmann, *J. Phys. Chem. B*, 1998, **102**, 2569–2577.
- 4 M. G. Martin and J. I. Siepmann, *J. Phys. Chem. B*, 1999, **103**, 4508–4517.
- 5 J. H. Cavka, S. Jakobsen, U. Olsbye, N. Guillou, C. Lamberti, S. Bordiga and K. P. Lillerud, *J. Am. Chem. Soc.*, 2008, **130**, 13850–13851.
- 6 A. K. Rappé, C. J. Casewit, K. S. Colwell, W. A. Goddard and W. M. Skiff, *J. Am. Chem. Soc.*, 1992, **114**, 10024–10035.
- 7 S. L. Mayo, B. D. Olafson and W. A. Goddard, *J. Phys. Chem.*, 1990, **94**, 8897–8909.